Chemistry of Metals and Alloys

Chem. Met. Alloys 13 (2020) 78-84
Ivan Franko National University of Lviv
www.chemetal-journal.org

Electrochemical hydrogenation of the $R_2Zn_{17-x}Mn_x$ phases (R = Y, La, Gd, Tb)

Nataliya CHORNA[1], Vasyl KORDAN[1]*, Vitalii NYTKA[1], Oksana ZELINSKA[1], Ivan TARASIUK[1], Anatoliy ZELINSKIY[1], Volodymyr PAVLYUK[1]

[1] *Department of Inorganic Chemistry, Ivan Franko National University of Lviv, Kyryla i Mefodiya St. 6, 79005 Lviv, Ukraine*
* *Corresponding author. E-mail: vasyl.kordan@lnu.edu.ua*

Received October 21, 2020; accepted December 29, 2020; available on-line January 4, 2021
https://doi.org/10.30970/cma13.0409

The electrochemical hydrogenation of the solid solutions $R_2Zn_{17-x}Mn_x$, x = 0.5-0.9 (R = Y, La, Gd, Tb) was studied in Ni-MH battery prototypes for the first time. Phase analysis of the electrode materials on the basis of these compounds was carried out before and after hydrogenation by X-ray powder diffraction, scanning electron microscopy, energy-dispersive X-ray spectroscopy, and X-ray fluorescence spectroscopy. All the majority phases crystallize in the hexagonal Th_2Ni_{17}-type structure. As electrodes the alloys showed similar electrochemical behavior and the amount of deintercalated hydrogen increased in the order La < Y < Gd < Tb. The largest degree of amorphization and formation of oxides, such as ZnO and R_2O_3, were observed for the Y- and La-containing alloys after 50 cycles of hydrogenation/dehydrogenation. The geometrically most advantageous sites are octahedral voids in Wyckoff position 6*h* of the initial structures with a coordination polyhedron [HR_2(Zn,Mn)$_4$] for the H-atom.

Solid solution / Th_2Ni_{17}-type structure / Electrochemical hydrogenation / Ni-MH battery

Introduction

Some intermetallic compounds based on rare-earth (R) and 3d-transition (T) metals demonstrate the ability to absorb and desorb reversibly large amounts of hydrogen. These phases are often called “hydrogen storage materials” and can be used for accumulation and storage of hydrogen and development of electrode materials for nickel-metal hydride batteries. The crystal structure of the phases is characterized by tetrahedral and octahedral voids suited for hydrogen insertion [1,2]. The best sorption characteristics are usually observed for materials developed on the basis of Laves phases and phases with the structure types of $CaCu_5$, $CeNi_3$, $PuNi_3$, Th_2Ni_{17}, Th_2Zn_{17}, Gd_2Co_7, Ce_2Ni_7, Mo_2FeB_2, W_2CoB_2 [3-14].

Previous investigations have shown that the phases with stoichiometry 2:17, having either rhombohedral Th_2Zn_{17}-type or hexagonal Th_2Ni_{17}-type structures, have significant void size [13,15,16] and affinity to hydrogen. The rhombohedral structure contains octahedral voids with a center in Wyckoff position 9*e* (½, 0, 0). Small atoms, such as C, N and H, can enter these voids, forming a superstructure with the $Ce_2Mn_{17}C_{1.77}$-type. The hexagonal Th_2Ni_{17}-type contains two voids suitable for intercalation: octahedral with the center in a site in Wyckoff position 6*h* (x, 2x, ¼) and tetrahedral with the center in a position 12*i* (x, 0, 0) [17]. In case of gas hydrogenation of the alloys, hydrides with two types of occupied void are formed. During electrochemical hydrogenation we assume that only octahedral voids are occupied by H-atoms, forming a superstructure with $Tb_2Mn_{17}C_{2.5}$-type (Fig. 1). The octahedral voids are the first to be occupied by H-atoms, forming a coordination polyhedron [HR_2M_4], because of geometrical and coordination reasons. The H-atoms have the same coordination in the $CaCu_5$-type structure [18]. Occupation of the tetrahedral voids with the center in a position 12*i* occurs only for higher H content (more than 3 H/f.u.).

The sorption ability and electrochemical properties of the electrode materials constructed on the basis of R_2T_{17} and RT_5 phases can be improved by doping the binary compounds with other elements. In our previous works [15,16,18,19] we confirmed the positive influence of *s*-, *p*- and *d*-elements on the electrochemical hydrogenation of the compounds Tb_2Ni_{17} and $TbCo_5$. Doping pure magnesium with lithium and aluminum promotes hydrogen desorption, improves corrosion resistance and hydrogen mobility into the solid phase of the electrode [20,21].

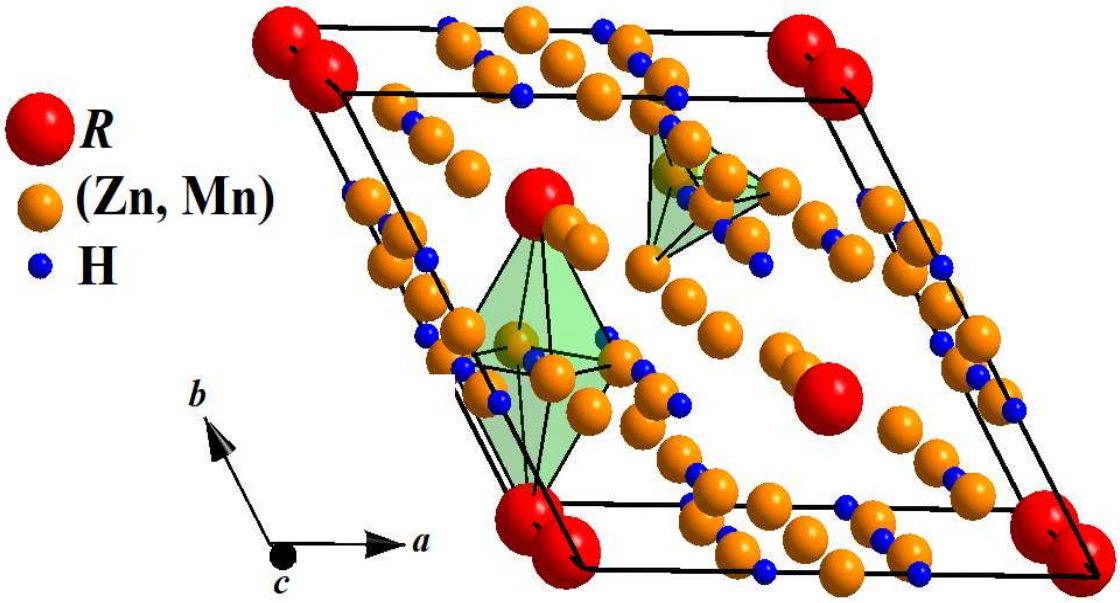

Fig. 1 Unit cell of $R_2Zn_{17-x}Mn_x$ hydrides ($Tb_2Mn_{17}C_{2.5}$-type structure) and coordination polyhedra for H-atoms at the centers of octahedral voids in 6*h* and at the centers of tetrahedral voids in 12*i*.

The purpose of this research was to study the electrochemical hydrogenation of solid solutions based on $R_2Zn_{17-x}Mn_x$ (R = Y, La, Gd, Tb) and to investigate changes of the compositions of the electrodes during electrochemical processes in a 6M KOH electrolyte environment.

Experimental

Yttrium, lanthanum, gadolinium, terbium, zinc, and manganese with nominal purities of more than 99.9 wt.% (commercial) were used as starting materials for the synthesis. Alloys with the nominal composition $R_{10.5}Zn_{84.5}Mn_5$ (R = Y, La, Gd, Tb) were prepared by arc melting of pressed pellets of pure components (excess of Zn was 10 wt.% and of Mn 2 wt.%) under a purified argon atmosphere. To reach homogeneity the samples were sealed in evacuated silica ampules, annealed at 500°C for four weeks and finally quenched in cold water.

Phase analysis of the samples was carried out before and after the electrochemical processes, using powder X-ray diffraction data collected on a diffractometer DRON-2.0M (Fe *K*α-radiation). Refinement of lattice parameters was carried out by the least-squares method using LATCON [22] and PowderCell [23] programs. X-ray fluorescence spectroscopy (analyzer ElvaX Pro) was used for the investigation of the compositions of the electrodes before and after hydrogenation. Qualitative and quantitative compositions of the observed phases were studied by energy-dispersive X-ray spectroscopy using a scanning electron microscope TESCAN Vega 3 LMU with the Oxford Instruments Aztec ONE system.

Electrochemical hydrogenation was carried out in two-electrode Swagelok-type cells. The battery prototype consisted of a negative electrode containing 0.2-0.3 g of the alloy and a positive electrode containing a mixture of dried $Ni(OH)_2$ with 10 wt.% of graphite (~0.5 g) added for better conductivity. A separator (pressed cellulose) soaked in 6M KOH electrolyte was placed between the electrodes to avoid contact between them. Chronopotentiograms of the Ni-MH battery prototypes were obtained in galvanostatic regime over 50 cycles of charge-discharge, using a galvanostat MTech G410-2 [24]. The amount of deintercalated hydrogen per formula unit (H/f.u.) of the studied electrodes was determined using Faraday's formula, where the H-content is directly proportional to the discharge time and inversely proportional to the amount of alloy. The electrochemical reactions that occur on the electrodes can be presented by the following scheme:

$$R_2Zn_{17-x}Mn_xH_y + yOH^- \underset{\text{charge (hydrogenation)}}{\overset{\text{discharge (dehydrogenation)}}{\rightleftharpoons}} R_2Zn_{17-x}Mn_x + yH_2O + y\bar{e}$$

$$yNiO(OH) + yH_2O + y\bar{e} \underset{\text{charge (oxidation)}}{\overset{\text{discharge (reduction)}}{\rightleftharpoons}} yNi(OH)_2 + yOH^-$$

Table 1 Lattice parameters of $R_2Zn_{17-x}Mn_x$ (R = Y, La, Gd, Tb) phases and their hydrides.

Composition	a, Å	c, Å	V, Å^3	$\Delta V/V$, %
$Y_2Zn_{17-x}Mn_x$	8.9714(9)	8.818(2)	614.6(1)	0.80
$Y_2Zn_{17-x}Mn_x\mathbf{H}_y$	8.982(1)	8.867(9)	619.5(6)	
$La_2Zn_{17-x}Mn_x$ [25]	9.118(2)	8.877(4)	639.3(3)	1.36
$La_2Zn_{17-x}Mn_x\mathbf{H}_y$	9.146(1)	8.944(3)	648.0(3)	
$Gd_2Zn_{17-x}Mn_x$ [25]	8.988(1)	8.811(2)	616.5(2)	0.63
$Gd_2Zn_{17-x}Mn_x\mathbf{H}_y$	8.9929(9)	8.858(2)	620.4(1)	
$Tb_2Zn_{17-x}Mn_x$	8.9924(9)	8.836(2)	618.8(1)	1.33
$Tb_2Zn_{17-x}Mn_x\mathbf{H}_y$	9.048(1)	8.844(1)	627.0(2)	

3. Results and discussion

The phase analysis of the $R_2Zn_{17-x}Mn_x$ (R = Y, La, Gd, Tb) alloys by X-ray diffraction confirmed that all the samples contained solid solutions with the expected hexagonal Th_2Ni_{17}-type structure. The Y- and La-containing alloys, in addition to the majority phases, also contained a small amount of rhombohedral 2:17 phases with a solubility of Mn of less than 4.5 at.%. For the La-containing alloy, trace amounts of a phase with 1:11 stoichiometry ($BaCd_{11}$-type structure) were observed. The Gd-containing sample was two-phase; besides the main $Gd_2Zn_{17-x}Mn_x$ phase, solid solutions on the basis of Zn were observed. The alloy with Y contained three phases: the hexagonal and rhombohedral modifications of the 2:17 phase and Zn. It is worth noticing that the changes of the unit-cell parameters of the investigated phases obey the effect of lanthanide contraction. After 50 charge-discharge cycles of the electrochemical hydrogenation the unit-cell volume of the phases, had increased as a result of the intercalation of hydrogen into the octahedral voids of the structure of the anode materials (see Table 1).

The SEM-images (back-scattered electrons mode) in Fig. 2 confirm the amounts of phases obtained by X-ray diffraction. The overall compositions ($Y_{12.9(6)}Mn_{4.5(7)}Zn_{82.6(9)}$, $La_{11.7(4)}Mn_{3.9(6)}Zn_{84.4(7)}$, $Gd_{9.6(3)}Mn_{3.5(5)}Zn_{86.9(8)}$, and $Tb_{11.8(6)}Mn_{4.2(8)}Zn_{84.0(6)}$) and elemental mapping of the studied alloys obtained from the EDX-analysis correlated well with the starting nominal compositions of the samples $R_{10.5}Mn_5Zn_{89.5}$.

More detailed analysis of the compositions of the electrodes was carried out using X-ray fluorescence spectroscopy. The X-ray fluorescence spectra and overall compositions of the electrode based on $Gd_{10.5}Mn_5Zn_{84.5}$, as an example, is presented in Fig. 3. Traces of oxygen and potassium from the electrolyte were removed by internal normalization of the data. We observed minor changes of composition, partial destruction of the crystal structure and enhanced grain etching of the samples that depend on the experimental conditions of hydrogenation. The composition of the initial sample changed from $Gd_{11.0}Mn_{4.4}Zn_{84.6}$ (Fig. 3*a*) to $Gd_{10.1}Mn_{4.8}Zn_{85.1}$ after 10 cycles of charge-discharge (Fig. 3*b*) and to $Gd_{9.2}Mn_{6.1}Zn_{84.7}$ after 50 cycles of charge-discharge (Fig. 3*c*), which was the main reason of the capacity loss. The corrosion resistance of the La- and Y-containing phases is the lowest and after the electrochemical studies the X-ray powder patterns showed a large content of lanthanum and zinc oxides. The difference between the X-ray powder patterns of the $La_2Zn_{17-x}Mn_x$ electrode sample before and after 50 cycles of hydrogenation-dehydrogenation is presented in Fig. 4. The appearance of a noticeable amorphous halo in the low-angle region also confirmed significant amorphization of the electrode material.

Here we selected an optimal current density at charging of 1.0 mA/cm^2 for 5 h in galvanostatic regime, because a larger current very quickly destroys the crystalline electrode and the amorphous electrode is oxidized to individual oxides. Similar experiments were carried out with electrodes based on $SmNi_5$ solid solutions [18]. Selected discharge curves with longer discharge time for the battery prototypes based on $R_2Zn_{17-x}Mn_x$ are presented in Fig. 5. During the first 7-15 cycles processes of surface and volume activation occurs. The longest discharge time was observed at the 7-th cycle for the La-containing electrode (0.68 H/f.u.), at the 8-th cycle for the Y-containing electrode (0.72 H/f.u.), at the 11-th cycle for the Gd-containing electrode (1.92 H/f.u.), and at the 14-th cycle for the Tb- containing electrode (1.94 H/f.u.). The maximum amount of intercalated hydrogen was not reached under the conditions of the experiment. Larger amounts of hydrogen can be obtained by gas hydrogenation at high pressure and temperature. Alloying of the Y- and La-containing phases by corrosion-resistant components such as Co, Ni, *etc.* might increase the corrosion resistance of the alloys, capacitive parameters and life cycle of the electrode material.

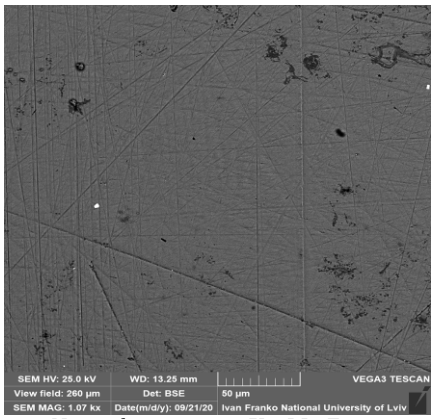

Nominal composition: $\mathbf{Y_{10.5}Mn_5Zn_{89.5}}$

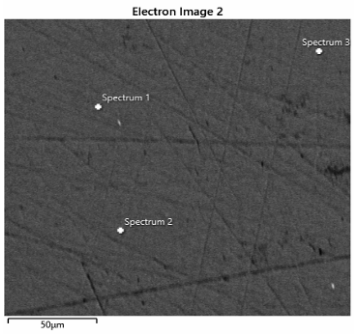

Spectrum 1–3 (main phase):
$\mathbf{Y_{12.9(6)}Mn_{4.5(7)}Zn_{82.6(9)}}$;
Black points:
~Zn

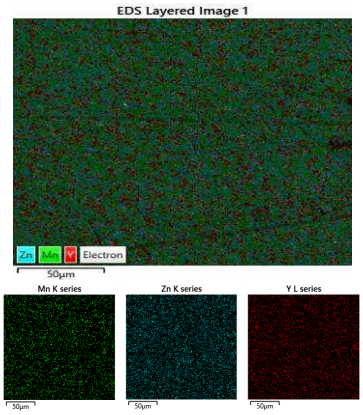

Integrated composition: $\mathbf{Y_{13.0}Mn_{3.7}Zn_{83.3}}$

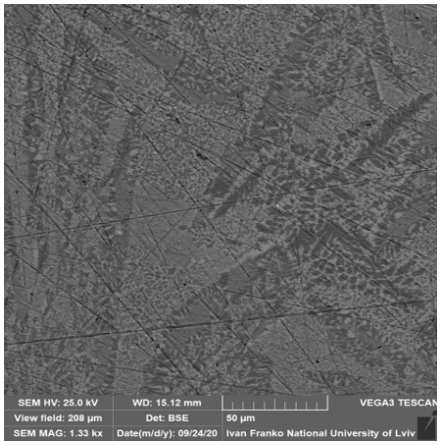

Nominal composition: $\mathbf{La_{10.5}Mn_5Zn_{89.5}}$

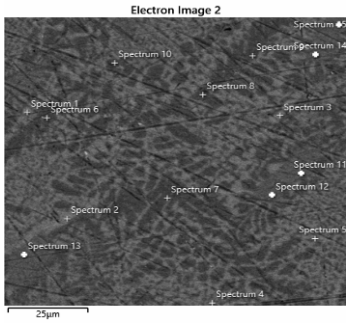

Spectrum 1–5 (light phase):
$\mathbf{La_{11.7(4)}Mn_{3.9(6)}Zn_{84.4(7)}}$;
Spectrum 6–10 (grey phase):
$\mathbf{La_{9.1(7)}Mn_{2.8(6)}Zn_{88.1(8)}}$;
Spectrum 11–15 (dark phase) 11-15:
$\mathbf{La_{2.1(6)}Mn_{1.8(5)}Zn_{96.1(9)}}$

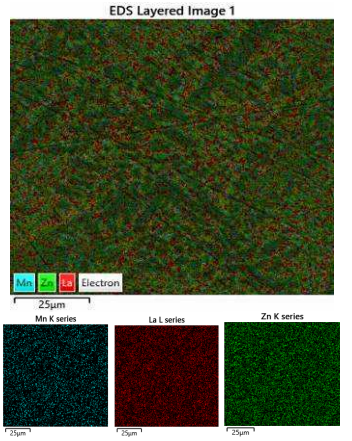

Integrated composition: $\mathbf{La_{11.2}Mn_{4.1}Zn_{84.7}}$

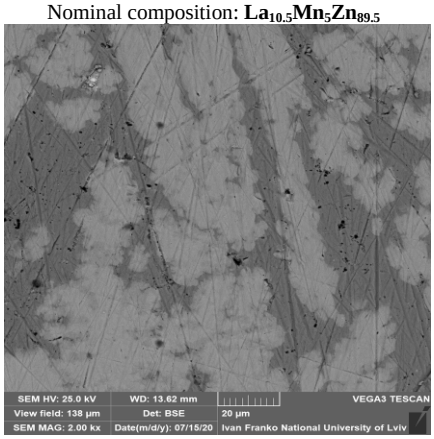

Nominal composition: $\mathbf{Gd_{10.5}Mn_5Zn_{89.5}}$

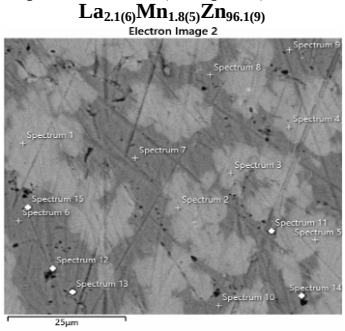

Spectrum 1–5 (light phase):
$\mathbf{Gd_{9.6(3)}Mn_{3.5(5)}Zn_{86.9(8)}}$;
Spectrum 6–10 (dark phase):
$\mathbf{Gd_{1.1(3)}Mn_{0.9(5)}Zn_{98.0(7)}}$;
Spectrum 11–15 (black points):
~ZnO

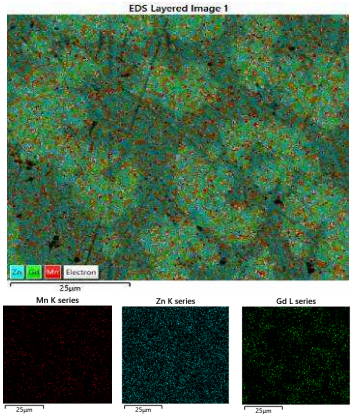

Integrated composition: $\mathbf{Gd_{8.9}Mn_{3.9}Zn_{87.2}}$

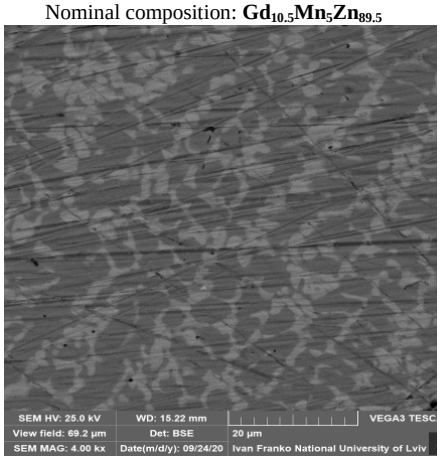

Nominal composition: $\mathbf{Tb_{10.5}Mn_5Zn_{89.5}}$

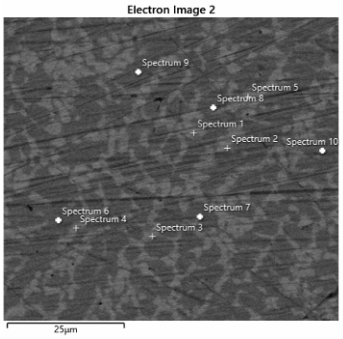

Spectrum 1–5 (light phase):
$\mathbf{Tb_{19.1(9)}Mn_{4.5(1.1)}Zn_{76.4(1.3)}}$;
Spectrum 6–10 (dark phase):
$\mathbf{Tb_{11.8(6)}Mn_{4.2(8)}Zn_{84.0(6)}}$

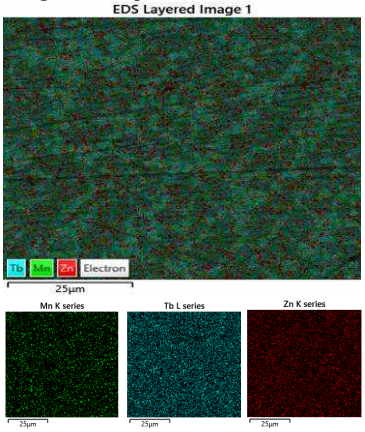

Integrated composition: $\mathbf{Tb_{13.0}Mn_{5.2}Zn_{81.8}}$

Fig. 2 Back-scattered electron images of the surfaces, phase compositions and elemental mapping of the studied alloys.

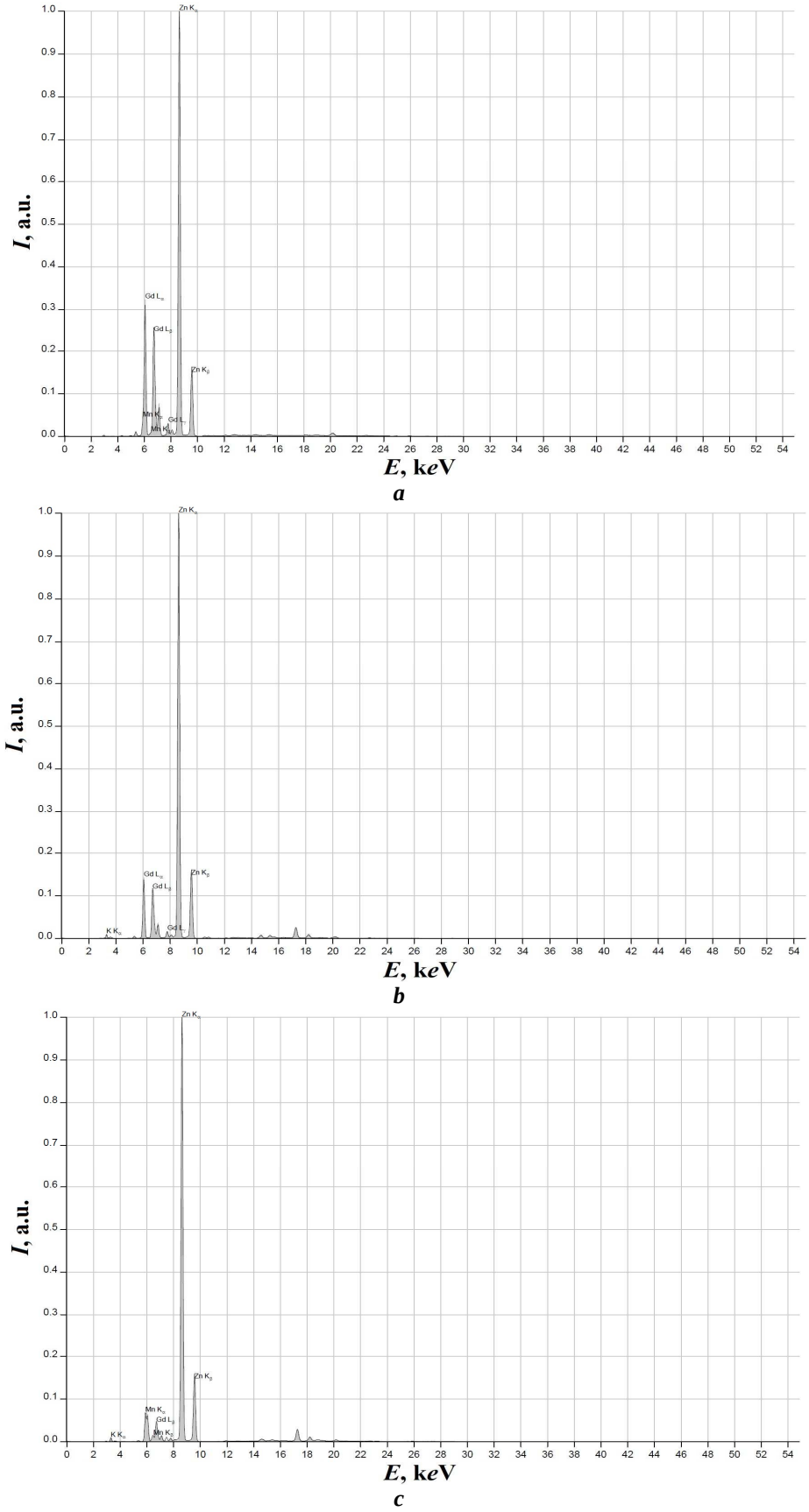

Fig. 3 X-ray fluorescence spectra of electrode based on $Gd_{10.5}Mn_5Zn_{84.5}$: initial (*a*), after 10 (*b*) and after 50 (*c*) charge-discharge cycles.

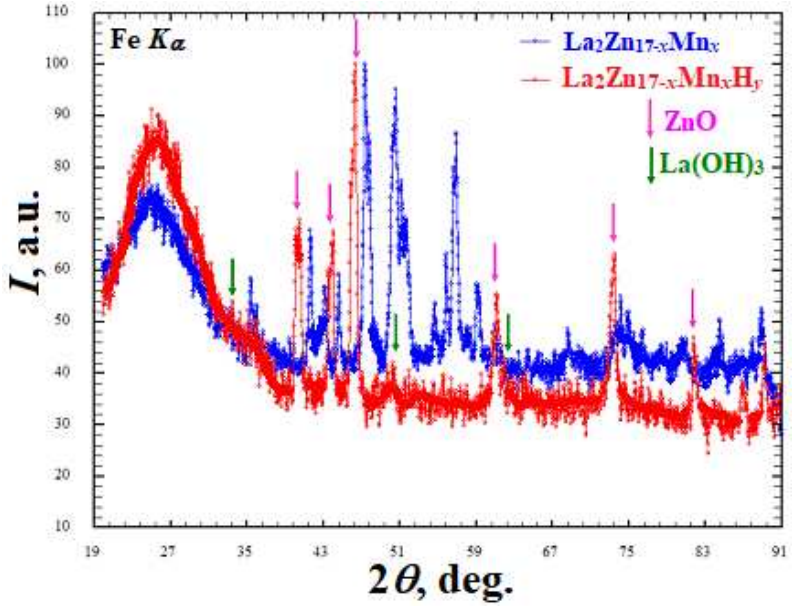

Fig. 4 X-ray powder patterns of $La_2Zn_{17-x}Mn_x$ before (blue profile) and after 50 cycles (red profile) of hydrogenation.

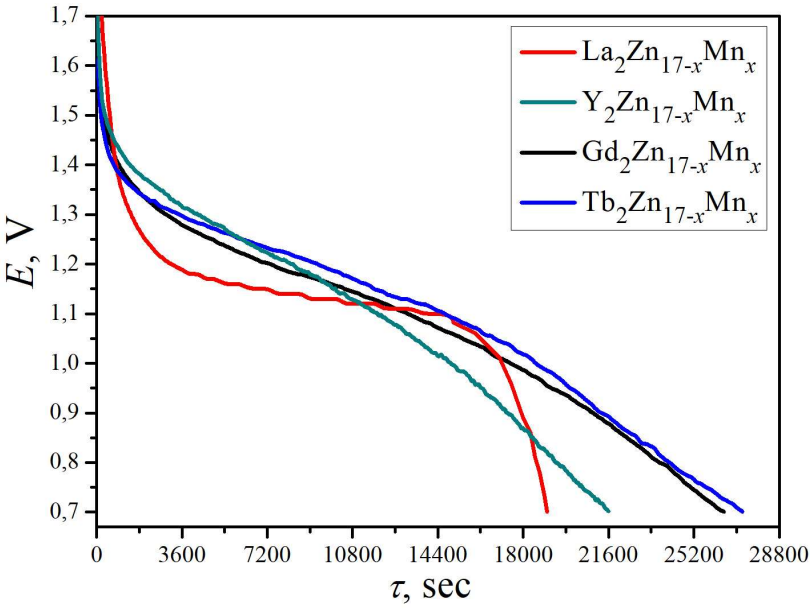

Fig. 5 Selected discharge curves for the battery prototypes based on $R_2Zn_{17-x}Mn_x$.

Conclusion

The $R_2Zn_{17-x}Mn_x$ (R = Y, La, Gd, Tb) phases crystallize in the hexagonal Th_2Ni_{17}-type structure. The solubility of Mn does not exceed 4.0-4.5 at.% (~0.5-0.9 Mn/f.u.). Besides the main phases, the Y- and La-containing alloys are characterized by the formation of trace amounts of rhombohedral 2:17 phase. According to the EDX-analysis, the solubility of Mn in these compounds is similar to that of the hexagonal phases. Such low solubility can be explained by differences in physical and chemical characteristics between zinc and manganese, while the atomic radii have close values. As electrodes the alloys demonstrated similar electrochemical behavior, the discharge time and amount of H/f.u. increased in the order La < Y < Gd < Tb. Under the experimental conditions the La-containing electrode incorporated

0.68 H/f.u., the Y-containing electrode 0.72 H/f.u., the Gd-containing electrode 1.92 H/f.u. and the Tb-containing electrode 1.94 H/f.u. For the Y- and La- alloys significant amorphization and etching by the electrolyte were observed.

Acknowledgements

This work was supported by the Ministry of Education and Science of Ukraine (grant No. 0118U003609).

References

[1] J.O. Besenhard, *Handbook of Battery Materials*, Wiley-VCH, Weinheim, Germany, 1999, 1023 p.
[2] C.A. Vincent, B. Scrosati, *Modern Batteries: An Introduction to Electrochemical Power Sources*, 2nd Ed., Arnold, London, 1997, 351 p.
[3] K. Miliyanchuk, L. Havela, R. Gladyshevskii, *Chem. Met. Alloys* 12(1/2) (2019) 16-20.
[4] N. Chorna, N. Sagan, O. Zelinska, V. Kordan, A. Zelinskiy, V. Pavlyuk, *Chem. Met. Alloys* 11(1/2) (2018) 27-33.
[5] K. Miliyanchuk, S. Maskova, L. Havela, R. Gladyshevskii, *Chem. Met. Alloys* 9(3/4) (2016) 169-173.
[6] A. Stetskiv, B. Rozdzynska-Kiełbik, G. Kowalczyk, W. Prochwicz, P. Siemion, V. Pavlyuk, *Solid State Sci*. 38 (2014) 35-41.
[7] K. Giza, W. Iwasieczko, V.V. Pavlyuk, H. Bala, H. Drulis, L. Adamczyk, *J. Alloys Compd*. 429 (2007) 352-356.
[8] L. Wang, H. Yuan, H. Yang, K. Zhou, D. Song, Y. Zhang, *J. Alloys Compd*. 302 (2000) 65-69.
[9] J.M. Joubert, M. Latroche, R.C. Bowman Jr., A. Percheron-Guégan, F. Bourée-Vigneron, *Appl. Phys. A* 74 (Suppl. 1) (2002) 1037-1039.
[10] K. Giza, W. Iwasieczko, V.V. Pavlyuk, H. Bala, H. Drulis, *J. Power Sources* 181 (2008) 38-40.
[11] S. De Negri, P. Solokha, A. Saccone, V. Pavlyuk, *Intermetallics* 16 (2008) 168-178.
[12] B. Rozdzynska-Kielbik, W. Iwasieczko, H. Drulis, V.V. Pavlyuk, H. Bala, *J. Alloys Compd*. 298 (2000) 237-243.
[13] V. Kordan, V. Nytka, I. Tarasiuk, O. Zelinska, R. Serkiz, V. Pavlyuk, *Visn. Lviv Univ., Ser. Khim*. 61(1) (2020) 80-92.
[14] N. Chorna, V. Andrash, O. Zelinska, V. Kordan, A. Zelinskiy, V. Pavlyuk, *Visn. Lviv Univ., Ser. Khim*. 59(1) (2018) 107-114.
[15] V. Kordan, V. Nytka, G. Kovalczyk, A. Balinska, O. Zelinska, R. Serkiz, V. Pavlyuk, *Chem. Met. Alloys* 10(2) (2017) 61-68.
[16] V. Kordan, O. Zelinska, V. Pavlyuk, V. Nytka, R. Serkiz, *Chem. Met. Alloys* 9(3/4) (2016) 153-157.
[17] O. Isnard, S. Miraglia, J.L. Soubeyroux, D. Fruchart, A. Stergiou, *J. Less-Common Met.* 162(2) (1990) 273-284.
[18] V. Kordan, I. Tarasiuk, I. Stetskiv, R. Serkiz, V. Pavlyuk, *Chem. Met. Alloys* 12(3/4) (2019) 77-87.
[19] I. Tarasiuk, I. Stetskiv, V. Kordan, V. Pavlyuk, *Visn. Lviv Univer., Ser. Khim*. 58(1) (2017) 117-123 (in Ukrainian).
[20] V. Pavlyuk, W. Ciesielski, N. Pavlyuk, D. Kulawik, M. Szyrej, B. Rozdzynska-Kielbik, V. Kordan, *Ionics* 25(6) (2018) 2701-2709.
[21] V. Pavlyuk, W. Ciesielski, N. Pavlyuk, D. Kulawik, G. Kowalczyk, A. Balińska, M. Szyrej, B. Rozdzynska-Kielbik, A. Folentarska, V. Kordan, *Mater. Chem. Phys.* 223 (2019) 503-511.
[22] G. King, D. Schwarzenbach, *Latcon. Xtal 3.7 System*, University of Western Australia, 2000.
[23] W. Kraus, G. Nolze, *Powder Cell for Windows*, Berlin, 1999.
[24] http://chem.lnu.edu.ua/mtech/mtech.htm.
[25] N. Chorna, V. Kordan, O. Zelinska, A. Zelinskiy, V. Pavlyuk, *Coll. Abstr. VI Ukr. Sci. Pract. Conf. Young Scient. Stud. "Physics and Chemistry of the Solid State: Status, Achievements and Prospects"*, Lutsk, 2016, p. 143-145.